

Breakup and atomization of a stretching crownIliia V. Roisman,^{*} Tatiana Gambaryan-Roisman, Olympia Kyriopoulos, Peter Stephan,[†] and Cam Tropea[‡]*Darmstadt University of Technology, Faculty of Mechanical and Process Engineering, Petersenstraße 30, 64287 Darmstadt, Germany*

(Received 12 December 2006; revised manuscript received 21 May 2007; published 7 August 2007)

This study is devoted to experimental and theoretical investigation of splash produced by spray impact onto a smooth, rigid target under microgravity conditions. In particular, the formation of a film by the deposited liquid, the propagation and breakup of uprising sheets created by drop impacts, and the creation of secondary droplets have been observed. Three scenarios of splash have been identified during the experiments: (i) cusp formation and jetting due to the rim transverse instability, (ii) sheet destruction and the consequent rapid axisymmetric capillary breakup of a free rim, and (iii) the rim merging. Experimental data for various geometrical parameters of splash have been collected. Next, in order to predict the typical length scales of the interjet distance, a linear stability analysis of the rim in relation to transverse disturbances has been performed. The influence of the sheet stretching has been investigated and shown to be significant. The experimentally measured average values of the interjet distances agree well with the theoretical predictions. The sheet stretching is responsible for the appearance of the relatively long interjet distances.

DOI: [10.1103/PhysRevE.76.026302](https://doi.org/10.1103/PhysRevE.76.026302)

PACS number(s): 47.20.Dr, 47.55.dr, 68.03.Cd

I. INTRODUCTION

This study is motivated by the problem of describing the hydrodynamics of spray impact onto a rigid wall. This phenomenon is an element of many industrial applications, such as spray painting, wetting, coating and encapsulation, spray forming, agriculture spray deposition, spray cooling and cleaning, and atomization based on spray impingement. Spray impact onto chamber walls is inevitable in small internal combustion engines and in systems for spray drying.

The prediction of the parameters of the secondary spray associated with spray impact is required for the design of the atomizers based on the spray-wall interaction principle—for example, the air blast atomizers for gas turbines. Moreover, knowledge about the secondary spray is necessary for developing a reliable model of spray cooling, which is one of the promising technologies for intensive cooling of high-power microelectronics, of human tissues, and of extremely hot metal slabs.

A spray impacting onto a rigid wall creates on its surface a thin fluctuating liquid layer. Images of the spray-initiated flows often look rather “chaotic” [1]. A large variety of phenomena in this liquid layer is initiated by single-drop impacts and their interactions. The observed phenomena include emerging and propagation of uprising sheets generated by impact of relatively large droplets, their breakup, crater formation in the film, emerging of jets, and capillary waves. If the typical impact velocity and the typical drop diameter are high enough, the sheets and jets become unstable; they break up and lead to the secondary liquid atomization and generation of the secondary spray. Many frequently observable splash scenarios have been recently distinguished and classified [2].

One widely used approach for the modeling of spray impact is based on the description of spray impact as a superposition of single-drop impacts onto a wetted or dry wall. A comprehensive review of such models can be found in [3]. One of the recent models of this art can be found in [4]. However, it has been shown [5] that none of these models can be used as a reliable and universal predictive tool since they do not agree well with the experimental data for wall impact of a real, polydisperse, dense spray.

The second approach frequently used in the description of spray painting (see, for example, [6]) neglects completely the inertial effects associated with the spray impact. Negative flux of secondary droplets and the momentum of the oscillations of the liquid in the film on the wall are also neglected. The spray is considered only as a source of liquid volume flux. Next, the motion of the deposited liquid film is described using the governing equations of hydrodynamics of falling films.

The third approach is based on direct numerical simulations of the spray impact. In Ref. [7] the spray impact has been simulated numerically using a commercially available numerical code, based on the volume-of-fluid method. Spray impact was modeled by simultaneous impact of 22 liquid drops randomly distributed in space above a rigid wall. Such computations have to account for a wide range of typical lengths and typical times. They are extremely expensive and still cannot be considered as a predictive tool for spray impact description.

Another semiempirical approach is based on the fitting of the extensive experimental data [5,8] obtained using the phase Doppler instrument. Such models are valid for a definite range of parameters used in these experiments, and the possibility of the generalization of such models remains questionable.

The only way to understand the hydrodynamics of spray impact is in the identification of elementary parts of the flow in the wall film and in their respective modeling. Among such elements, the impact of a single drop onto a dry wall or onto a stationary uniform liquid film has been investigated most intensively, starting from the well-known study of Wor-

^{*}roisman@sla.tu-darmstadt.de; URL: <http://www.sla.tu-darmstadt.de/roisman/sprayportal/DI.htm>

[†]URL: <http://www.tu-darmstadt.de/fb/mb/ttd/>

[‡]URL: <http://www.sla.tu-darmstadt.de>

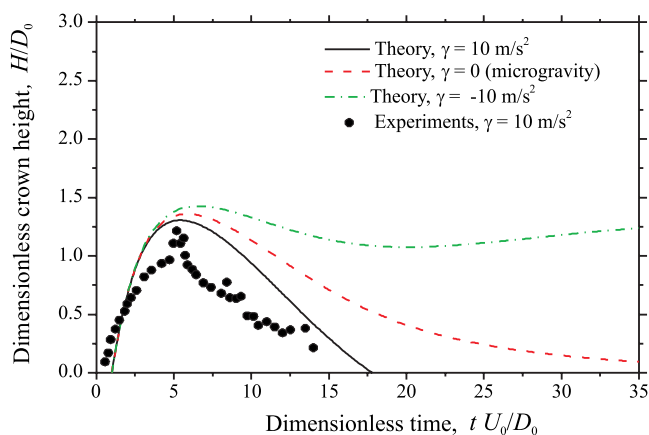


FIG. 1. (Color online) The height of the crown: the comparison of the theory [14] with the experimental data for the terrestrial, microgravity conditions and reversed configuration.

thington [9] more than 130 years ago. Detailed reviews of drop impact studies can be found in [10,11] and elsewhere.

The mechanism of formation of free uprising sheets due to drop impact is presently well understood. These sheets appear as a result of the interaction of two inertia-dominated film flows with different velocities. This phenomenon has been modeled theoretically in application to a normal drop impact in [12], where the film flow has been approximated using the concept of propagation of a kinematic discontinuity. Next, it has been shown [13] that the influence of viscosity on the crown propagation is not very significant if the impact Reynolds number is high. This approach was later generalized in [14] for arbitrary geometries and applied to a description of the propagation of the crown formed by normal or oblique single-drop impact onto a uniform liquid film.

Any free liquid sheet (including those formed by spray impact) is bounded by a free rim. The rim formation is caused by capillary forces, and the mechanism of this formation is well known [15]. The surface tension applied to the rim is balanced by the inertia of the flow entering into it from the sheet. The rim relative velocity has been accounted for in a theoretical description of a single-drop impact onto a uniform liquid wall film [14]. In Fig. 1 an example for the comparison of theoretical predictions with experimental data [16] for the crown height as a function of dimensionless time is shown. The impact parameters are $We = \rho D_0 U_0^2 / \gamma = 296$, $h_{film}/D_0 = 0.29$. Here D_0 and U_0 are the initial drop diameter and impact velocity, We is the impact Weber number, h_{film} is the initial undisturbed film thickness, and ρ and γ are the liquid density and surface tension. The theory agrees well with the experiments under terrestrial conditions ($g = 10 \text{ m/s}^2$). Additionally, in Fig. 1 the theoretical predictions for the crown height under microgravity conditions, $g = 0$, and in reversed configuration, $g = -10 \text{ m/s}^2$, are shown. The influence of gravity on the maximum crown height is only minor whereas the time of crown propagation is influenced significantly by the gravity magnitude and direction. Moreover, in the reversed configuration, the capillary forces are small in comparison with the gravity and the crown does not “fall” back onto a wetted wall. This result is relevant to the present study since our experiments of spray impact have

been performed under microgravity conditions during a parabolic flight campaign.

One of the most challenging problems related to an understanding of splash is the rim stability. For some conditions the rim remains stable and falls down onto the wall without the appearance of any visible disturbances. If the drop impact velocity exceeds the splash threshold [17], the rim transverse instability [2] leads to the appearance of cusps and jets [12]. These jets then break up and generate secondary drops. A description of the jet breakup mechanism can be found in [18,19]. Understanding the origin of the rim breakup is necessary for a description of liquid atomization [20] and the formation of secondary spray.

The mechanism of the breakup is described by the linear stability analysis of the rim to the transverse disturbances of its centerline [2]. A typical length scale of this instability is comparable with the breakup length of an infinite liquid cylinder atomized due to the capillary instability. This fact has been already recognized by some researchers [21,22].

The present paper is aimed at an investigation of the mechanism of splash produced by spray impact. This study includes experimental observations of the shape of the liquid film and recognition of various modes of atomization. It is focused on a detailed description of the atomization process: the rim diameters, the distances between fingerlike jets, the jet diameters, and the diameters of the secondary drops.

One of our goals is to show theoretically that the rim instability leading to the crown splash is not caused by the Rayleigh capillary instability, although it is related to it. The origin of the rim instability is the moment of forces produced by the inertia of the liquid entering the rim from the free liquid sheet. Many parameters and factors influence the phenomena of rim breakup. In the present paper the analysis is aimed at an investigation of film stretching. This stretching can explain the appearance of relatively long stable pieces of the rim, observed in the experiments.

The paper is organized as follows. In Sec. II the experimental setup and the measurement methods are described. In Sec. III the observed phenomena of spray impact and the corresponding fluctuating flow in the wall film and its breakup and atomization are discussed. In particular, three scenarios of splash have been identified and described: corona splash, splash due to the film breakup and rim detachment, and the emergence of single, vertical bifurcating jets through corona merging.

In Sec. IV the rim instability is analyzed. The influence of the stretching of the free sheet is emphasized. In Sec. V the results of the measurements of the various geometrical parameters relevant to the secondary atomization are given and compared with the corresponding typical dimensions obtained from the linear stability analysis. In Sec. VI concluding remarks are given.

II. EXPERIMENTAL METHOD

In order to understand the mechanism of secondary atomization, the spray impact onto a rigid target and the resulting near-wall flow have been experimentally investigated. The experimental setup, shown in Fig. 2, includes five major sub-

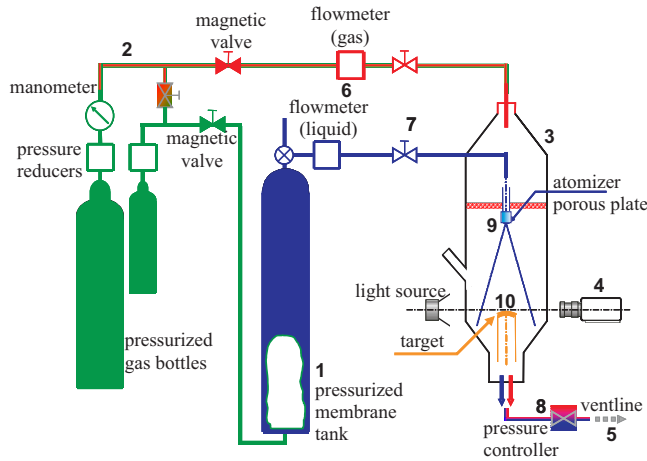


FIG. 2. (Color online) Sketch of the experimental setup.

systems: liquid supply system including a pressurized membrane tank (1) provides water for spray generation, gas supply system (2) allows one to ventilate the test cell (3) by a gas co-flow, optical visualization system (4), electronic measurement and control system (not shown in this figure), and the extraction system (5) aimed at exhausting the deposited liquid and gas from the test cell.

The volumetric rates of water and gas are measured and controlled using the measurement devices (6). These rates can be varied by changing the injection pressure in the supply line (7). The pressure inside the experimental cell is kept constant at 0.8 bar (8).

The spray of distilled water is generated by a full-cone pressure swirl atomizer (9) (Spraying Systems 30° series) installed in the test cell at the distance of 70 mm from a target (10). The volumetric rate is varied in the range 0.25–0.5 l/min which corresponds to the injection pressure in the range 0.35–2.5 bar.

The curved surface of the target is a truncated sphere with the diameter of the projected area 20 mm. The convex spherical shape of the surface has been chosen to allow a precise observation of the profile of the film generated by spray impact at the target generatrix.

The spray impact has been observed using a high-speed video system consisting of a light source and a CMOS camera. The spray-wall interaction has been captured with a frame rate of 8000 fps. This frame rate allows several stages of the same splash event to be observed. The resolution of the images is 20 μm per pixel; the total field of view is 10.9 × 2.7 mm. The optical access to the region of spray impact has been enabled by the system of transparent windows. The surfaces of the windows have been treated to achieve a superhydrophobic effect aimed at preventing the deposition of the drops on the windows.

The experiments have been performed under microgravity conditions during a parabolic flight campaign. The images of the near-wall film have been processed, and important characteristics relevant to splash (rim diameter, interfinger distances, diameters of secondary drops) have been evaluated.

III. WALL FILM OBSERVATIONS

The high-speed video system allows detailed observations of the dynamics of the wall film flow. These observations

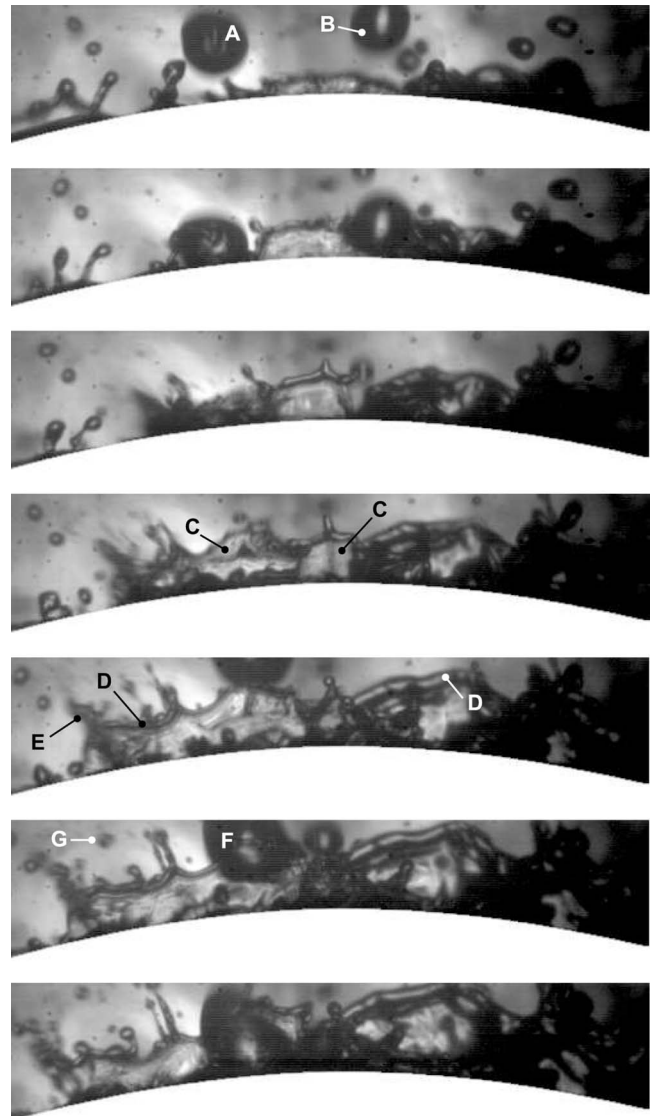


FIG. 3. Typical time sequence of spray impact with multiple, nonsymmetric splashes. The spherical target image is shown white. A: drop of 1.1 mm in diameter impacting with the velocity 6 m/s. B: drop of 1 mm in diameter impacting with the velocity 4.9 m/s. C: uprisings. D: free rims. E: fingerlike jets. F: third impacting drop. G: secondary drops.

help us to better understand the phenomena and to identify possible ways of their modeling. Despite the wide variety of events occurring during spray impact, only three main types of splash leading to the film-rim breakup and creation of secondary drops have been identified.

A typical short-time sequence of spray impact obtained using the high-speed video system is shown in Fig. 3. In this sequence the film produced by spray impact can be clearly seen since the profile of the spherical substrate is marked in white. In the upper three frames single-drop impacts can be clearly seen. The drop creates uprising, crownlike, free liquid sheets. The rim formed at the edge of the sheets, the cusps at the rim, and the jets can be easily identified on the images.

However, during the spray impact other events can also be observed. An example of such an event is shown in Fig. 4. In

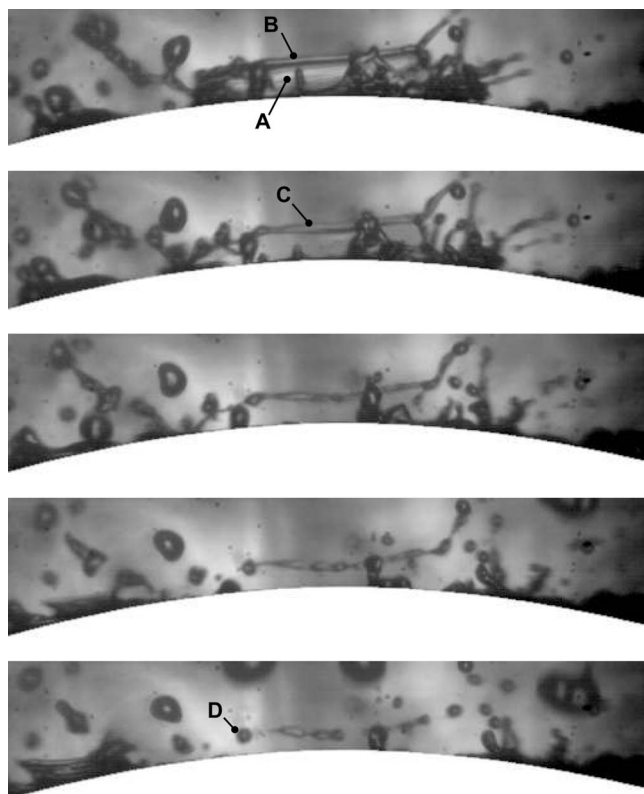


FIG. 4. Example of splash produced after the breakup of a free sheet. *A*: free uprising sheet. *B*: rim. *C*: free jet formed after the rim detachment and sheet breakup. *D*: secondary droplets formed after the capillary breakup of a jet.

this time sequence the breakup of a free sheet can be observed. This breakup leads to the detachment of a rim (see the second frame) which is actually a free-floating almost-circular jet. This rim then immediately breaks up into several drops. The mechanism of this breakup is caused by the capillary instability of a liquid jet [23,24] which is already well understood. Note, however, that this breakup is nearly axisymmetric. No significant rim bending or cusp or jet formation can be observed. It is obvious that the conventional mechanism of rim breakup shown in Fig. 3 is completely different.

It should be noted that we have never observed the phenomena shown in Fig. 4 in spray impact under terrestrial conditions, whereas free jets created by the rim detachment from the free sheet can be frequently observed under microgravity conditions. The reason for this is in the much longer duration of the crown propagation under μg conditions. This propagation is accompanied by significant sheet thinning which increases the probability of breakup (see the prediction in Fig. 1).

We would like to emphasize that in our case gravity forces (or lack of) do not significantly influence the breakup mechanism but change the duration of the crown propagation, allowing several modes of breakup to appear.

Similar phenomena for rim detachment have been observed during the interaction of two drops on a wall [25]. Such an interaction leads to the emergence of an uprising liquid sheet whose lifetime is much longer than the crown

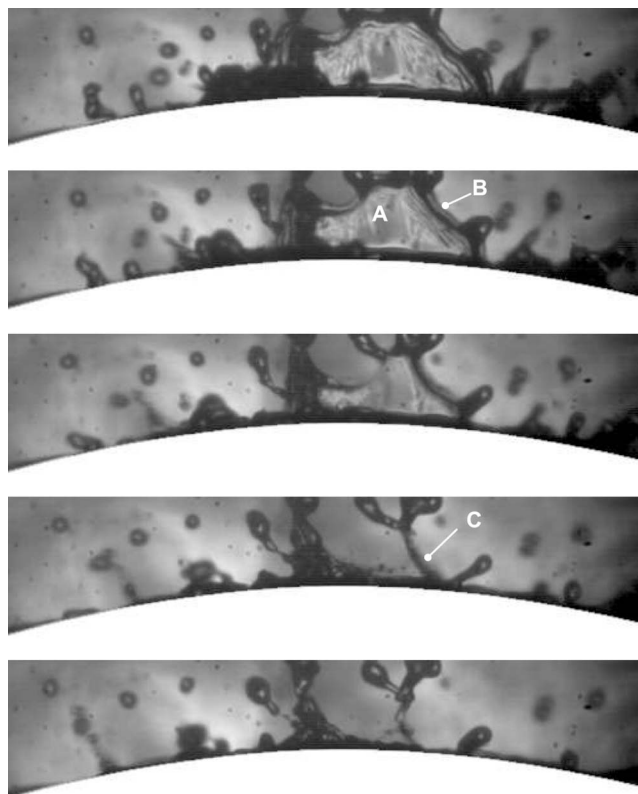


FIG. 5. Example of splash leading to the formation of the jets emerging directly from the wall film. *A*: uprising sheet. *B*: rim. *C*: single bifurcating jet.

emerged due to a single-drop impact (see, for example, the analysis of such drop interactions in [26]).

The third splash scenario observed in our spray impact experiments is illustrated in Fig. 5. In these images the detailed mechanism of formation of bifurcating jets can be easily seen. Such bifurcating jets have been observed earlier, but the mechanism of their formation was not clear. From the analysis of the time sequence in Fig. 5 it becomes evident that bifurcating jets are formed by the collapse of the rim bounding a nonsymmetric crown.

Note that in Fig. 5 the rim between the cusps is not straight. These observations contradict theoretical predictions obtained in [12,14]. The reason for the curved shape of the rim centerline can be the stretching of the free sheet. This stretching appears due to the nonuniform speed of the sheet propagation [12].

The effect of sheet stretching on the rim stability is analyzed theoretically in the next section.

IV. RIM BENDING INSTABILITY

We have observed that the most frequent reason for splash accompanied by the formation of jets and secondary drops is the rim transverse instability. The rim is formed at the edge of a free liquid sheet due to capillary forces [15].

The rim stability is influenced by several factors, such as surface tension, viscosity, rim acceleration, rim-to-sheet size ratio, curvature of the rim centerline, velocity and thickness

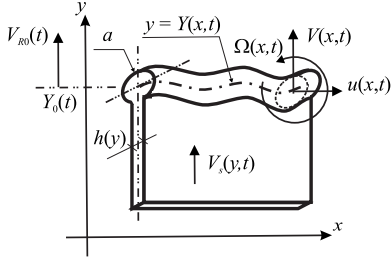


FIG. 6. Rim bounding a free liquid sheet. (a) Propagation of a straight undisturbed rim and (b) development of small disturbances of the rim centerline.

gradients in the sheet, etc. The rim instability can be enhanced by the sheet fluctuations and by the aerodynamic forces.

A consensus on the mechanism of the rim breakup has not been yet achieved. Therefore, the most relevant approach is to consider the simplest case of dynamics of the rim, bounding a planar and uniform free liquid sheet.

As shown in Figs. 3–5, the centerline of the rim bends always in the plane of the free film and the emerging finger-like jets are almost parallel to this plane. Therefore, the influences of the forces, associated with the rim acceleration in the direction normal to the sheet, and of the capillary centripetal forces, related to the curvature of the rim centerline, are small and can be neglected.

In Ref. [2] the influences of the relative sheet thickness and of the rim acceleration have been investigated. The theory predicts that over a wide range of influencing parameters the typical length of the most unstable wave is in the range 4–5 of the rim diameter. This length is almost not influenced by the rim-to-sheet size ratio and by the rim acceleration.

The length of the most unstable wave by rim breakup is very similar to the length of the most unstable axisymmetric capillary wave on the cylindrical jet. However, the mechanisms of these two instabilities are completely different. The transverse rim instability is caused by the inertia of the liquid entering the rim. In particular, the moment of the forces generated by this flow is the main origin of the rim bending.

In the present study the analysis is focused on the influence of the sheet stretching in the direction normal to the rim. This effect can explain the appearance of the relatively long pieces of undisturbed rim observed in many time sequences during our experimental study.

A. Dynamics of a nearly straight rim: Long-wave approximation

Consider a Cartesian coordinate system $\{x, y\}$ with base vectors $\{e_x, e_y\}$, as shown in Fig. 6. Consider also a nearly straight rim bounding a free, nonviscous planar sheet of thickness $h(y, t)$. Denote the velocity of the liquid in the sheet as $V_S = V_S(y, t)e_y$. The flow in the film is directed along the y axis.

The median surface of the film, defined as $y = Y(x, t)$, resides in the plane $\{x, y\}$. Denote the radius of the rim cross section as $a(x, t)$, the cross-sectional area of the rim as

$A(x, t) = \pi a^2$, the moment of inertia of the rim cross section as $I(x, t) = \pi a^4/4$, and the velocity of the liquid in the rim as $V(x, t) = u(x, t)e_x + V(x, t)e_y$.

In the present analysis we assume small transverse long-wave disturbances of a nearly straight rim of the form

$$Y(x, t) = Y_0(t) + \epsilon(x, t), \quad a(x, t) = a_0(t) + \alpha(x, t),$$

$$V(x, t) = V_{R0}(t) + \epsilon_t(x, t), \quad (1)$$

where the functions ϵ and α , as well as the longitudinal velocity u , are small.

The propagation of the rim centerline and the corresponding flow can be described using the quasi-one-dimensional approach [2] of rim dynamics. The governing equations are obtained modifying the theory for the dynamics of a circular jet [27,28] and accounting for the capillary force and the inertia effects related to the interaction between the rim and the free sheet. The linearized mass balance, the axial momentum balance, and the moment of momentum balance equations of the rim can be obtained by neglecting the second-order small terms:

$$\frac{\partial A}{\partial t} + A_0 \frac{\partial u}{\partial x} - h(V_S - V) = 0, \quad (2a)$$

$$\rho A_0 \frac{\partial u}{\partial t} - \frac{\partial P}{\partial x} - f_S \cdot e_x = 0, \quad (2b)$$

$$\rho A \frac{\partial V}{\partial t} - P\kappa - \frac{\partial Q}{\partial x} - f_S \cdot e_y = 0, \quad (2c)$$

$$\rho \frac{\partial}{\partial t}(I_0 \Omega) - \frac{\partial M}{\partial x} Q - m_S = 0, \quad (2d)$$

where ρ is the liquid density, κ is the curvature of the centerline of the rim, f_S is the distributed external force per unit length of the rim associated with the free sheet, m_S is the distributed moment of the external forces f_S , P is the magnitude of the longitudinal tensile force and Q is the shear force in the transverse direction applied to the cross section of the rim, $\Omega = \partial V / \partial x$ is the angular velocity of the rim cross section, and M is the moment of stresses in the cross section.

The linearized expressions for the longitudinal force P , for the distributed force f_S , and for the moment m_S accounting for the surface tension and the inertia of the liquid entering the rim can be written in the following form:

$$P = \pi \gamma a + \gamma A_0 \frac{\partial^2 a}{\partial x^2}, \quad (3a)$$

$$f_S = [\rho h(V_S - V)^2 - 2\gamma]e_y + \left[-\rho h(V_S - V)u + 2\gamma \frac{\partial Y}{\partial x} \right]e_x, \quad (3b)$$

$$m_S = -\rho h a_0 (V_{S0} - V_{R0})u, \quad (3c)$$

at $y = Y$, where γ is the surface tension coefficient.

The moment of stresses, M , appears when the gradient of the stresses in the rim cross section is significant due to rim

acceleration. It was shown in [2] that rim acceleration only slightly influences the length of the most unstable mode. In the present work only the cases of relatively small rim acceleration are considered such that the term M is assumed to be negligibly small. The expression for the shear force Q is not given explicitly as a function of the geometry and the velocity of the rim. It can be obtained from the system of equations (2).

The equation for the propagation of the rim centerline is

$$\frac{\partial Y}{\partial t} = V. \quad (4)$$

B. Base solution: Motion of a straight rim

In the case of the propagation of a straight uniform rim the set of governing equations (2)–(4) can be reduced to the well-known form which was first obtained in [15]:

$$\frac{dA_0}{dt} = h(V_{S0} - V_{R0}), \quad (5a)$$

$$A_0 \dot{V}_{R0} = h(V_{S0} - V_{R0})^2 - \frac{2\gamma}{\rho}, \quad (5b)$$

$$\frac{dY_0}{dt} = V_{R0}, \quad (5c)$$

where $\dot{V}_{R0} = dV_{R0}/dt$ is the rim acceleration.

It can be shown that in the case of a uniform sheet of constant and uniform velocity the remote asymptotic solution of Eq. (5) leads to the well-known equation for the rim relative velocity:

$$V_{S0} - V_{R0} = \sqrt{\frac{2\gamma}{\rho h}}. \quad (6)$$

C. Small disturbances of the rim centerline

Consider now small disturbances of the rim defined in Eqs. (1). The linearized equations for these small disturbances can be written with the help of Eqs. (2) in the following form:

$$2\pi a_0 \alpha_t + A_0 u_x + h(\epsilon_t - S\epsilon) = 0, \quad (7a)$$

$$-\rho A_0 u_t + \pi \gamma \alpha_x + \gamma A_0 \alpha_{xxx} - W_0 u + 2\gamma \epsilon_x = 0, \quad (7b)$$

$$-\rho A_0 \epsilon_{tt} + \pi \gamma a_0 \epsilon_{xx} + Q_x + 2W_0(S\epsilon - \epsilon_t) = 0, \quad (7c)$$

$$2\rho I_0 \epsilon_{xt} + \rho \frac{dI_0}{dt} \epsilon_{xt} + a_0 W_0 u - Q = 0, \quad (7d)$$

where $W_0 = \rho h(V_{S0} - V_{R0})$ is the volume flux of the liquid entering the rim and $S = \partial V_S / \partial y$ is the local velocity gradient in the free sheet (rate of stretching) at $y = Y_0$.

The set of linear differential equations (7) with time-dependent coefficients can be simplified assuming that the

instability growth rate is much higher than the rate of change of the rim radius. Then the expressions for a_0 , A_0 , and I_0 can be assumed to be “frozen” in time. In this case the following form of the disturbances can be assumed:

$$\epsilon = \epsilon_0 \exp(\omega t + i\xi x), \quad \alpha = \alpha_0 \exp(\omega t + i\xi x),$$

$$u = u_0 \exp(\omega t + i\xi x), \quad Q = q_0 \exp(\omega t + i\xi x), \quad (8)$$

where ω is the growth rate of disturbances and $\xi = 2\pi/\ell$ is the wave number (ℓ being the disturbance wavelength).

Introducing the disturbances (8) into the system (7), we obtain the following characteristic equation:

$$\mathbf{A} \cdot \mathbf{b} = 0, \quad (9)$$

where

$$\mathbf{A} = \begin{pmatrix} 2\pi a_0 \omega & A_0 i \xi & h(\omega - S) & 0 \\ A_{21} & -W_0 - \rho A_0 \omega & 2\gamma i \xi & 0 \\ 0 & 0 & A_{33} & i \xi \\ 0 & a_0 W_0 & A_{43} & -1 \end{pmatrix}, \quad (10a)$$

$$\mathbf{b} = (\alpha_0 \ u_0 \ \epsilon_0 \ q_0)^T, \quad (10b)$$

and

$$A_{21} = \pi \gamma i \xi - \gamma A_0 i \xi^3, \quad (10c)$$

$$A_{33} = -\rho A_0 \omega^2 - \xi^2 \pi \gamma a_0 - 2W_0(\omega - S), \quad (10d)$$

$$A_{43} = 2\rho I_0 \omega^2 i \xi + \frac{a_0^2 W_0}{2} \omega i \xi. \quad (10e)$$

The dispersion equation for small bending disturbances is

$$\det(\mathbf{A}) = 0. \quad (11)$$

Next, the following scales are used to write the problem in dimensionless form:

$$\omega = \sqrt{\frac{\gamma}{\rho a_0^3}} \bar{\omega}, \quad S = \sqrt{\frac{\gamma}{\rho a_0^3}} \bar{S}, \quad \xi = \bar{\xi} / a_0,$$

$$h = \bar{h} a_0, \quad W_0 = \bar{W}_0 \sqrt{\rho \gamma a_0}. \quad (12)$$

The dimensionless dispersion relation takes the following form:

$$\begin{aligned} & 2(2 + \bar{\xi}^2) \pi^2 \bar{\omega}^4 + 4(3 + \bar{\xi}^2) \pi \bar{W}_0 \bar{\omega}^3 \\ & + [(2(4 + \bar{\xi}^2) \bar{W}_0^2 - 8\bar{S} \pi \bar{W}_0 + \pi^2 \bar{\xi}^2 (2 + \bar{\xi}^2 + \bar{\xi}^4))] \bar{\omega}^2 \\ & + [-8\bar{S} \bar{W}_0 + \{8 + 2\bar{h}(\bar{\xi}^2 - 1) + \pi \bar{\xi}^2 (3 + \bar{\xi}^2)\} \bar{\xi}^2] \bar{W}_0 \bar{\omega} \\ & + 2\bar{\xi}^2 (\bar{\xi}^2 - 1) [-\bar{S}(\bar{h} + 2\pi) \bar{W}_0 + \pi^2 \bar{\xi}^2] = 0. \end{aligned} \quad (13)$$

Equation (13) for $\bar{\omega}$ is similar to the dispersion relation obtained in [2] but contains also terms associated with the sheet stretching. This equation has an analytical solution for four of its roots. The relatively long expressions for these roots are not given here. It is clear that only positive values of the real part of these solutions (associated with the rim

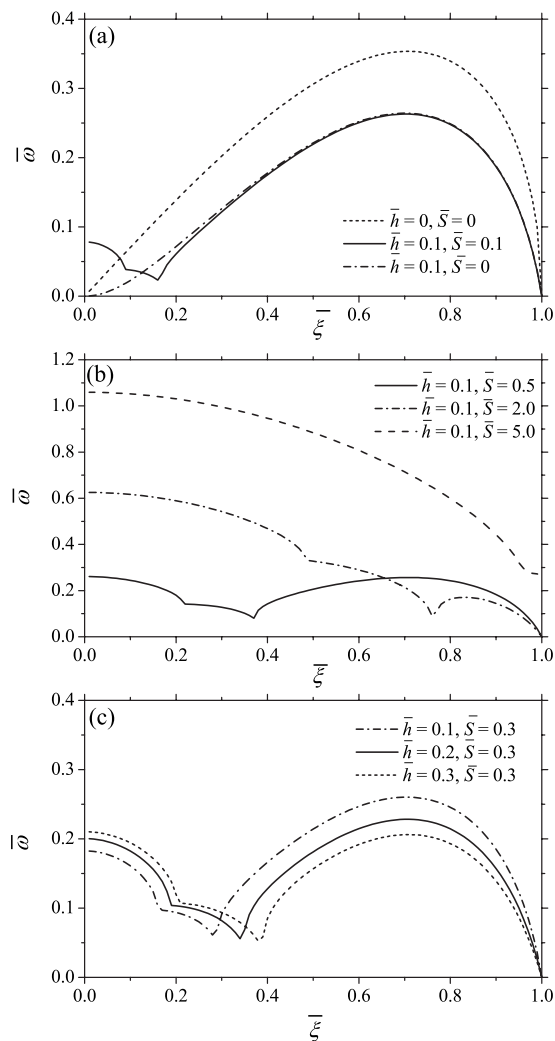


FIG. 7. Transverse rim instability: the rate of the disturbance growth as a function of the capillary number. (a) The effect of the relatively small stretching rate, (b) the effect of the relatively high stretching rate, and (c) the effect of the sheet thickness.

bending instability) are relevant. The results of the stability analysis are discussed in the next section.

V. RESULTS AND DISCUSSIONS

The relation between the disturbance growth rate and the disturbance wave number is shown in Fig. 7. In Fig. 7(a) these functions are compared with the case $\bar{h}=0$, $\bar{S}=0$, corresponding to the capillary breakup of a circular jet, and with the case $\bar{h}=0.1$, $\bar{S}=0$, corresponding to the instability of a rim bounding liquid sheet having a uniform velocity. It has been already shown in [2] that the rim is much more stable than a free circular jet of the same radius. It is seen that the disturbance growth rate in the presence of the liquid sheet ($\bar{h}=0.1$) is lower than the one in the case of a free rim ($\bar{h}=0$). The effect of the sheet stretching is significant only at small values of $\bar{\xi}$, and it manifests itself in the appearance of a maximum at $\bar{\xi}=0$. The wave number corresponding to the

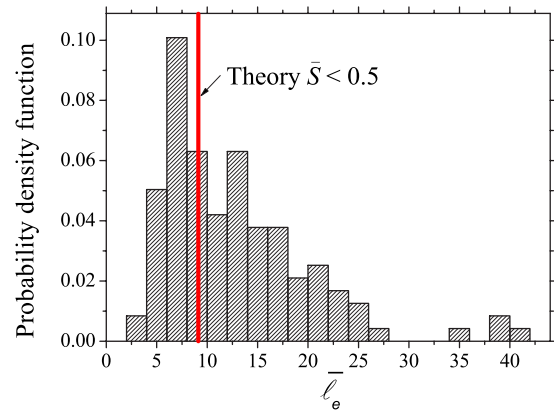


FIG. 8. (Color online) Distribution of the measured dimensionless interfinger distance $\bar{\ell}_e$.

fastest growing disturbance is similar for all three cases.

In Fig. 7(b) three cases with higher values of \bar{S} are considered. At $\bar{S}=0.5$ the value of $\bar{\omega}$ at small wave numbers is comparable with the maximum value at $\bar{\xi}=0.7$. At higher values of the dimensionless stretching parameter \bar{S} the instability at small $\bar{\xi}$ becomes dominant. This maximum is related to the fact that at small wave numbers (or longer wavelengths) the effect of surface tension, which is a primary stabilizing mechanism of the stretching sheet instability, is very weak.

The results shown in Fig. 7(c) indicate that increasing the relative film thickness \bar{h} leads to the stabilization of the rim in the range $0.4 < \bar{\xi} < 1$ and to the destabilization of the longest waves corresponding to the small wave numbers $\bar{\xi}$.

In order to validate the theoretical predictions, the splash events observed in the experiments have been analyzed. Data on the distance between fingerlike jets, their diameter, and rim diameter have been collected. In Fig. 8 the distribution of the dimensionless interfinger distance $\bar{\ell}_e$ is shown. This distance has been scaled by the rim radius (estimated as a half of the rim diameter). The predicted wavelength of the fastest growing disturbance for small \bar{S} is $\bar{\ell}_{theory} \approx 9$. The average experimental value is $\bar{\ell}_e \approx 12$, and the most probable value is $\bar{\ell}_e \approx 8$. The agreement is rather good.

In several events rims with relatively long interfinger distances have been registered (see Fig. 8, $33 < \bar{\ell}_e < 42$, corresponding to $0.15 < \bar{\xi} < 0.19$). Following the results shown in Fig. 7(b) this region corresponds to the rim breakup influenced by the sheet stretching.

At this point it is important to discuss whether the sheet stretching in the phenomena observed in our experiments is significant. The typical velocity in the sheet and its height are comparable with the impact velocity U_0 and the initial diameter D_0 of the impacting drop. It was shown in experiments [1] that the crown stops spreading at some time instant. It can be explained by the viscous damping of the flow in the thin internal film. Direct experimental evidence of this damping, resulting in an almost steady residual liquid film on the substrate, can be found in a recent paper [29]. The velocity in

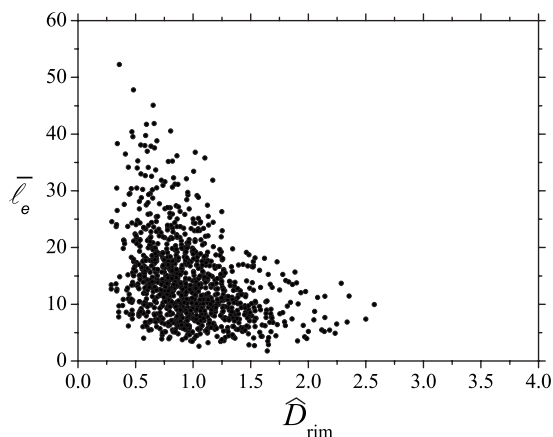


FIG. 9. The measured interfinger distance $\bar{\ell}_e$ as a function of the scaled rim diameter.

the sheet at the wall surface also vanishes at this time instant. The velocity gradient can be estimated as $S \sim U_0/D_0$. The dimensionless stretching parameter can be then determined with the help of Eqs. (12) as $S \sim \text{We}^{1/2}(a_0/D_0)^{3/2}$, where $\text{We} = \rho D_0 U_0^2 / \gamma$ is the impact Weber number.

In the spray shown in Figs. 3–5 the Weber number is $\text{We} \sim 350$. The rim radius to the drop diameter ratio is in the range of 0.05–0.1. The estimated dimensionless stretching is therefore $\bar{S} \sim 0.2$ –0.6. Following our theoretical analysis, at these values of \bar{S} the sheet stretching influences significantly the rim stability [see Fig. 7(b)].

Note also that the rim and sheet elongational stretching can also influence significantly the rim stability and the length of the most unstable wave [30]. Such elongational stretching is caused by the expansion of the diameter of the uprising crown. However, the relatively long free jet created by the rim detachment (shown in Fig. 4) almost does not change its length in time. The elongational stretching of this jet is probably not very significant.

In our experiments the spray parameters have been varied by changing the injection pressure. The average diameters and velocities of the impacting drops also change with the injection pressure. The average rim diameter $D_{\text{ra}} = 2a_0$ varies in the range from 80 to 190 μm . We introduce here the dimensionless rim diameter \hat{D}_{rim} scaled by D_{ra} . In Fig. 9 the measured dimensionless interjet distance $\bar{\ell}_e$ is shown as a function of the scaled rim diameter \hat{D}_{rim} . The length of the interjet distance increases with decreasing of \hat{D}_{rim} . The small values of \hat{D}_{rim} can be associated with the rims generated by the impact of relatively small drops. Moreover, the values of \hat{D}_{rim} are small at the early stages of the rim formation, when the ratio between the film thickness and the rim radius \bar{h} is large. The theoretical results shown in Fig. 7(c) predict a tendency towards a longer interjet distance, corresponding to smaller wave numbers, at higher values of \bar{h} . These predictions are therefore consistent with the experimental results.

The values of the diameter of the fingerlike jets correlate well with the rim diameter (see the distribution in Fig. 10). The average of their ratio is 1.2 whereas the theory [2] pre-

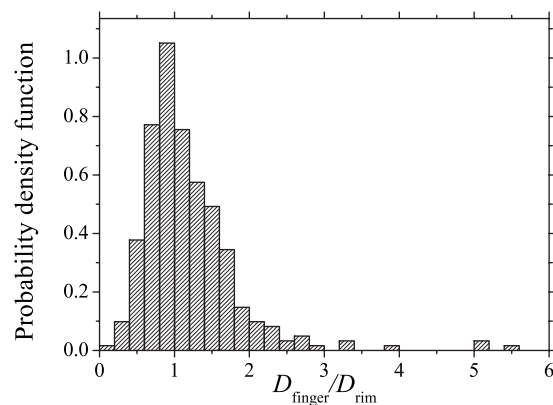


FIG. 10. Distribution of the dimensionless finger diameters.

dicts 1.22. This is again in good agreement between the theory and the experiment.

One logical conclusion from the present analysis is the assumption that the value of the secondary drop diameters can be also best scaled by the rim diameter. In our experiments the average of the ratio of these values is 1.5. The measured probability density function for the distribution of the drop-to-rim diameter ratio is shown in Fig. 11.

It should be noted that an accurate theoretical description and numerical simulation of splash and secondary atomization are rather complicated problems. Therefore, the empirical results shown in Fig. 11 can be very valuable in spray impact modeling.

VI. CONCLUSIONS

Three scenarios of splash produced during spray impact in microgravity are identified. The first splash scenario is similar to the well-known splash produced by a single-drop impact onto a stationary uniform liquid film [16]. A rim centerline is unstable to the bending disturbances. This instability leads to the formations of cusps and jets. These fingerlike jets generate a number of secondary droplets. The second splash scenario occurs when the rim detaches from the sheet. The free rim then breaks up due to the capillary instability of the cylinder to the axisymmetric disturbances of its radius.

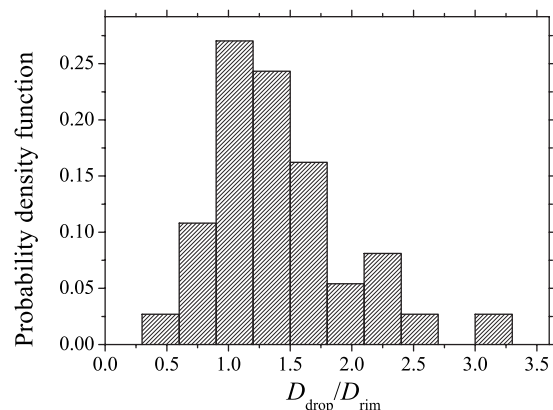


FIG. 11. Distribution of the dimensionless secondary drop diameter, scaled by the rim diameter.

The third splash scenario leads to the formation of single or multiple jets based on the target surface, which appeared as a result of rim bending and merging. Some of these jets can have a fascinating bifurcating form.

A linear stability analysis of a straight rim shows that the main origin of the transverse instability is the inertia of the liquid entering the rim. Capillary forces lead to a stabilization of this type of instability. This is the main difference between the mechanism considered in this study and the classical axisymmetric mode of the capillary instability of a cylindrical jet. The stretching of the sheet in a direction normal to the rim can effect significantly the rim stability. The stability analysis predicts the length of the most unstable wave to be $\ell \approx 9a_0$. These predictions agree well with the experimental data.

In some cases, however, the interjet distance is much higher than that predicted by the theory [2]. In the present

paper this effect is explained by the film stretching.

ACKNOWLEDGMENTS

The work has been performed in the framework of the research grant of BMWI “Sprayaufprall auf beheizte Oberflächen unter Mikrogravitation/Spray impact onto a heated surface under microgravity conditions” (Grant No. 50WM0635). The microgravity experiments have been performed during the 44th ESA parabolic flight campaign. The team would like to thank F. Gai (NOVESPAC) for technical help during the campaign. The authors would like to thank the German Science Foundation (DFG) for financial support in the framework of the Emmy Noether Program (Grant No. GA 736/2-3) and in the framework of the Collaborative Research Center 568 (TP A1).

-
- [1] D. Sivakumar and C. Tropea, *Phys. Fluids* **14**, L85 (2002).
 [2] I. V. Roisman, K. Horvat, and C. Tropea, *Phys. Fluids* **18**, 102104 (2006).
 [3] G. E. Cossali, M. Marengo, and M. Santini, *Atomization Sprays* **15**, 699 (2005).
 [4] S. S. Yoon, P. E. DesJardin, C. Presser, J. C. Hewson, and C. T. Avedisian, *Int. J. Multiphase Flow* **32**, 132 (2006).
 [5] C. Tropea and I. V. Roisman, *Atomization Sprays* **10**, 387 (2000).
 [6] M. H. Eres and L. W. Schwartz, in *ECS'2001—Proceedings of the 4th European Coating Symposium, Advances in Coating Processes*, Brussels, 2001, edited by J.-M. Buchlin and J. Anthoine (ULB&VKI, Brussels, 2001).
 [7] C. Böhm, D. A. Weiss, and C. Tropea, in *Proceedings of the 16th Annual Conference on Liquid Atomization and Spray Systems, ILASS-Europe*, Darmstadt, 2000, edited by C. Tropea and K. Heukelbach (SLA, TU Darmstadt, 2000), pp. VII.7.1–VII.7.6.
 [8] M. R. O. Panão and A. L. N. Moreira, *Exp. Fluids* **39**, 364 (2005).
 [9] A. M. Worthington, *Proc. R. Soc. London, Ser. A* **25**, 261 (1876).
 [10] M. Rein, *Fluid Dyn. Res.* **12**, 61 (1993).
 [11] A. Yarin, *Annu. Rev. Fluid Mech.* **38**, 159 (2006).
 [12] A. L. Yarin and D. A. Weiss, *J. Fluid Mech.* **283**, 141 (1995).
 [13] M. F. Trujillo and C. F. Lee, *Phys. Fluids* **13**, 2503 (2001).
 [14] I. V. Roisman and C. Tropea, *J. Fluid Mech.* **472**, 373 (2002).
 [15] G. I. Taylor, *Proc. R. Soc. London, Ser. A* **263**, 296 (1959).
 [16] G. E. Cossali, M. Marengo, A. Coghe, and S. Zhdanov, *Exp. Fluids* **36**, 888 (2004).
 [17] C. Mundo, M. Sommerfeld, and C. Tropea, *Atomization Sprays* **8**, 625 (1998).
 [18] J. Eggers, *Rev. Mod. Phys.* **69**, 865 (1997).
 [19] P. Marmottant and E. Villermaux, *Phys. Fluids* **16**, 2732 (2004).
 [20] C. J. Clark and N. Dombrowski, *J. Aerosol Sci.* **3**, 173 (1972).
 [21] J. W. M. Bush and A. E. Hasha, *J. Fluid Mech.* **511**, 285 (2004).
 [22] É. Reyssat and D. Quéré, *Europhys. Lett.* **76**, 236242 (2006).
 [23] Lord Rayleigh, *The Theory of Sound* (Macmillan, London, 1894).
 [24] C. Weber, *Z. Angew. Math. Mech.* **2**, 136 (1931).
 [25] G. E. Cossali, M. Marengo, and M. Santini, in *Proceedings of the 19th International Conference on Liquid Atomization and Spray Systems, ILASS-Europe*, Nottingham, 2004, edited by B. J. Azzopardi (School of Chemical, Environmental and Mining Engineering, University of Nottingham, Nottingham, 2004).
 [26] I. V. Roisman, B. Prunet-Foch, C. Tropea, and M. Vignes-Adler, *J. Colloid Interface Sci.* **256**, 396 (2002).
 [27] V. M. Entov and A. L. Yarin, *J. Fluid Mech.* **140**, 91 (1984).
 [28] A. L. Yarin, *Free Liquid Jets and Films: Hydrodynamics and Rheology* (Longman & Wiley, Harlow, New York, 1993).
 [29] S. Bakshi, I. V. Roisman, and C. Tropea, *Phys. Fluids* **19**, 032102 (2007).
 [30] D. V. Khakhar and J. M. Ottino, *Int. J. Multiphase Flow* **13**, 71 (1987).